Minimal Encounter Time and Separation Determine Ligand-Receptor Binding in Cell Adhesion

Philippe Robert,[†§] Alice Nicolas,[‡] Said Aranda-Espinoza,[†] Pierre Bongrand,[†§] and Laurent Limozin[†*]
[†]Adhesion & Inflammation, INSERM UMR 600 and Centre National de la Recherche Scientifique UMR 6212, Aix-Marseille University, Campus Luminy, Marseille, France; [‡]Laboratory of Technologies of Microelectronics, Centre National de la Recherche Scientifique UMR 5129, University of Grenoble 1, Grenoble, France; and [§]Assistance Publique des Hopitaux de Marseille, Marseille, France

ABSTRACT The binding properties of biomolecules play a crucial role in many biological phenomena, especially cell adhesion. Whereas the attachment kinetics of soluble proteins is considered well known, complex behavior arises when protein molecules are bound to the cell membrane. We probe the hidden kinetics of ligand-receptor bond formation using single-molecule flow chamber assays and Brownian dynamics simulations. We show that, consistent with our recently proposed hypothesis, association requires a minimum duration of contact between the reactive species. In our experiments, ICAM-1 anchored on a flat substrate binds to anti-ICAM-1 coated onto flowing microbeads. The interaction potential between bead and substrate is measured by microinterferometry and is used as an ingredient to simulate bead movement. Our simulation calculates the duration of ligand-receptor contacts imposed by the bead movement. We quantitatively predict the reduction of adhesion probability measured for shorter tether length of the ligand or if a repulsive hyaluronan layer is added onto the surface. To account for our results, we propose that bond formation may occur in our system by crossing of a diffusive plateau in the energy landscape, on the timescale of 5 ms and an energy barrier of 5 k_BT, before reaching the first detectable bound state. Our results show how to relate cell-scale behavior to the combined information of molecular reactivity and biomolecule submicron-scale environment.

INTRODUCTION

Cell-cell adhesion is mediated by the specific binding of adhesion molecules located on the opposed cell membranes. The kinetics of attachment and detachment play a crucial role in the adhesive function and often, initial adhesion is mediated by a single ligand-receptor bond (1). For more than a decade, kinetic studies of adhesion molecules concentrated on the detachment of single bonds (2), but studies of bond formation remain scarce and elusive (3–5). Such studies are rendered complicated by the fact that the receptors are attached to surfaces, which have to be brought into proximity before the establishment of molecular binding. Moreover, the cell surface is enriched with long dangling chains forming a steric repulsive barrier called the glycocalyx (6). Hence, in addition to the nature of the reactive site, the length and flexibility of the tethering part of the molecules have been shown to play a role in bond formation (7,8).

In this article, an antigen-antibody model is used for kinetic studies of surface-bound adhesion molecules. Some important physiological situations involve binding of cell surface-linked antibodies to pathogens' surface antigens. For example, B lymphocyte's encounter with its specific target determines its activation and antibody production. This is also the case for mastocytes and basophil polymorphonuclear cells, on which depend many antiparasitic defenses and allergy symptoms. Data of antigen-antibody interaction kinetics in surface-bound conditions are thus relevant to understanding immune response (9).

In the context of surface-bound reactants, in addition to the influence of the molecular environment, the notion of adhesion on-rate itself can be questioned (10). First, as recognized long ago by Bell (11), before binding, a diffusion-limited phase is necessary to bring the reactive sites into contact. Whereas for soluble species diffusion is difficult to control as an independent parameter, it is necessarily modified in case of surface-bound sites. Second, noncovalent bonds display various binding states, as exemplified by the fact that variable forces are required for their detachment (12,13). Therefore, it is difficult to define unambiguously the bound state. In this context, we have recently proposed that the classical framework of on-rate reaction may not be warranted in the case of surface-attached molecules. Although classical kinetics assumes that the bond formation probability depends on encounter time t_e as

$$P(t_e) \sim 1 - \exp(-k_{on}t_e),$$

we have proposed that, for certain attached molecules, a minimum duration t_{on} may be required to form a bond, writing the binding probability (14) as

$$P(t_e) \sim \mathrm{erfc}\sqrt{(t_{on}/t_e)}.$$

In this article, we examine this hypothesis in more detail by systematically varying the conditions of bond formation. We measure the frequency of arrest of microbeads coated with receptors (anti-ICAM-1) on a substrate coated with ligands (ICAM-1) in the presence of a shear flow. Experimental conditions are chosen to ensure that single-bond-mediated attachments dominate. The velocity of the beads,

Submitted September 9, 2010, and accepted for publication April 4, 2011.

*Correspondence: laurent.limozin@inserm.fr

Editor: Reinhard Lipowsky.

0006-3495/11/06/2642/10 $2.00

doi: 10.1016/j.bpj.2011.04.011

their distance to the surface (controlled by glycocalyx-like adsorbed polymer layer), and molecular tether length (through intermediate antibody) are varied.

To relate experimental parameters to molecular quantities, we implemented a dedicated Brownian simulation of bead motion. In addition to the information provided by the pioneering work of Chang and Hammer (15) and by more recent simulations from the literature (16–18), our simulation determines the duration of interaction between reactive species with the aim of comparing different binding kinetics. The number of bonds formed can be described with satisfactory accuracy as the product of a geometry-dependent number of molecular encounters and an efficiency of binding fixed by the encounter duration. This binding efficiency is well accounted for by defining a minimal time t_{on} for binding. In contrast, a binding efficiency proportional to the encounter duration, as classically assumed for soluble molecules by the use of on-rate k_{on}, does not account for the data. The experimentally observed dependence of frequency of adhesion on molecular tether length is quantitatively predicted by our model. Finally, the antiadhesive effect of the glycocalyx-like polymer layer is also predicted.

MATERIALS AND METHODS

Beads and surface functionalization

Coating of beads and substrates are designed to probe the interaction of ICAM-1 and an anti-ICAM-1 antibody, as previously described in Robert et al. (19). In brief, tosylactivated M450 Dynabeads (diameter 4.5 μm, density 1.5, CV 2% by flow cytometry; Invitrogen, Carlsbad, CA) were functionalized first with anti-mouse Fc fragment antibody (Serotec, Cergy-St-Christophe, France) and then with mouse anti-human ICAM-1 antibody (clone HA58; Ebioscience, San Diego, CA) or with the corresponding isotype control mouse antibody (mouse $IgG_{1,\kappa}$; Ebioscience). Such coating with two successive antibodies is referred to hereafter as double-layer configuration (DL). Alternatively, the first layer of antibody was omitted (single-layer configuration, SL) to reduce the extension of the molecular tether anchoring the binding site to the bead surface (Fig. 1).

For functionalization with Fc-ICAM-1 chimera, clean glass coverslips were incubated successively with Poly-L-lysine (300 kDa at 100 μg/mL in phosphate-buffered saline (PBS) during 30 min; Sigma-Aldrich, St. Louis, MO), glutaraldehyde (2.5% v/v in PBS, 30 min; Sigma-Aldrich), mouse anti-human Fc antibody in PBS (1 μg/mL, 30 min), and a blocking solution of 0.2 M glycine (Sigma-Aldrich) in 0.1 M phosphate buffer, pH 7.2 for 1 h. They were rinsed after each binding step and further incubated in human Fc-ICAM-1 chimera (R & D Systems Europe, Lille, France) solution for 30 min at different concentrations varying between 0.005 and 0.02 μg/mL. Coverslips were then rinsed in PBS and passivated in 10 mg/mL bovine serum albumin solution in PBS, or incubated in hyaluronic acid (700 kDa; Sigma-Aldrich) solution in PBS (concentration up to 0.2 μg/mL) then rinsed in PBS and finally passivated in 10 mg/mL bovine serum albumin solution in PBS.

The density of Fc-ICAM-1 molecules grafted on the substrate was estimated by measuring the fluorescence after direct labeling with a fluorescent antibody of the same isotype (HA58-phycoerythrin; Ebioscience). The surface density after incubation of Fc-ICAM-1 at the typical concentration of 0.01 μg/mL during 30 min was estimated at ~2 molecules/μm^2.

The length of the molecular tether was calculated taking a size of 4 nm for the immunology domain and assuming that the dangling Fc-ICAM-1 could be fully elongated in solution, whereas antibodies directly attached to the surfaces may be partly stuck parallel to the substrate (see Fig. 1). Thus the total tether length L was estimated to vary between 60 and 76 nm in DL configuration (three antibodies + Fc-ICAM-1) (14) and between 44 and 60 nm for the SL configuration (two antibodies + Fc-ICAM-1) (Fig. 1). Additionally, antibody molecules possess a central hinge allowing full rotation between the Fab and the Fc fragments, which are themselves relatively rigid (20); rotation is also possible between the Fc tag and the ICAM-1 fragment of the chimera (see the Supporting Material).

Measurements of single-molecule mediated bead arrests in flow

The frequency of arrests was measured using a flow chamber as already described in the literature (14,19). The shear rate was varied between 10 and 85 s^{-1}. Briefly, beads carried by the flow were observed on a fixed field of view under the microscope at ×20 magnification. Images were recorded with 20-ms time resolution. A bead was considered as arrested if its position did not change by more than $\delta x = 0.5$ μm in $\tau = 0.2$ s, and if its velocity before the arrest corresponded to that of a moving sedimented bead (19). The trajectory of at least 1000 beads, leading to up to ~500 arrests, were tracked for each experimental condition. The frequency of arrests (FA) was calculated as the ratio of number of arrests divided by the total displacement of the sedimented moving beads. An arrest was considered to continue as long as the arrest criterion was satisfied. Then, an apparent duration of arrest d_{app} could be measured. The true arrest duration d_{true} was obtained with the correction $d_{true} = d_{\mathrm{app}} + \tau - 2\delta x/v$, where v is the most probable velocity of the beads (19). The detachment curve was built by plotting the fraction of arrests exceeding the duration t as a function of t.

The adhesion of functionalized M450 beads to the underlying substrate coated with Fc-ICAM-1 was studied for various hyaluronic acid (HA) coverages. Positive adhesion assay was performed using M450 coated with anti-ICAM-1 antibody. Negative assay was performed on the same substrate with beads coated with a control isotype antibody. Specific adhesion frequency was defined as positive minus negative frequencies (19). The conditions for single bond formation and rupture were determined as follows. Successive dilutions of Fc-ICAM-1 on the substrate were performed until a point was reached where specific adhesion frequency varied proportionally with the Fc-ICAM-1 density. This occurred at an incubation concentration [Fc-ICAM-1] $\leq$ 0.01 μg/mL. In this regime, the detachment curves showed no variation with further Fc-ICAM-1 dilution, indicating that the nature of the bond rupture remained identical.

Measurements of bead-substrate interaction potential with RICM

Reflection interference contrast microscopy (RICM) (21) was used to measure the height of the beads above the substrate in the presence or absence of flow and for various hyaluronan coatings (19,22). Sequences of images obtained with the usual RICM setup (21) were recorded using either an iXon camera (Andor, Belfast, UK) or a GE480 (Prosilica, Vancouver, Canada), both run with a custom-built software under LABVIEW (National Instruments, Nanterre, France). The illumination numerical aperture was set at INA = 0.32 and illuminating wavelength was filtered at 546 ± 6 nm. The typical frame rate used was 50 Hz, and the typical exposure time was 20 ms.

The focus was established by maximizing the contrast of the field diaphragm, using a piezoelectric-controlled movement of the objective. Simultaneous sharpness of the diaphragm at three different points was obtained by manual adjustment of three corresponding screws under the stage and ensured a deviation from horizontality of the sample with respect to the (vertical) optical axis of $<10^{-3}$ rad. The retrieval of bead height from the radius of circular fringes was performed using the calibration established in a previous study (19). The histogram of bead height distribution $\Phi(z)$ was used to deduce the bead-surface potential $U(z)$ in the form $\Phi(z) \sim \exp(-U(z)/k_BT)$, with z the gap between the bead and the wall.

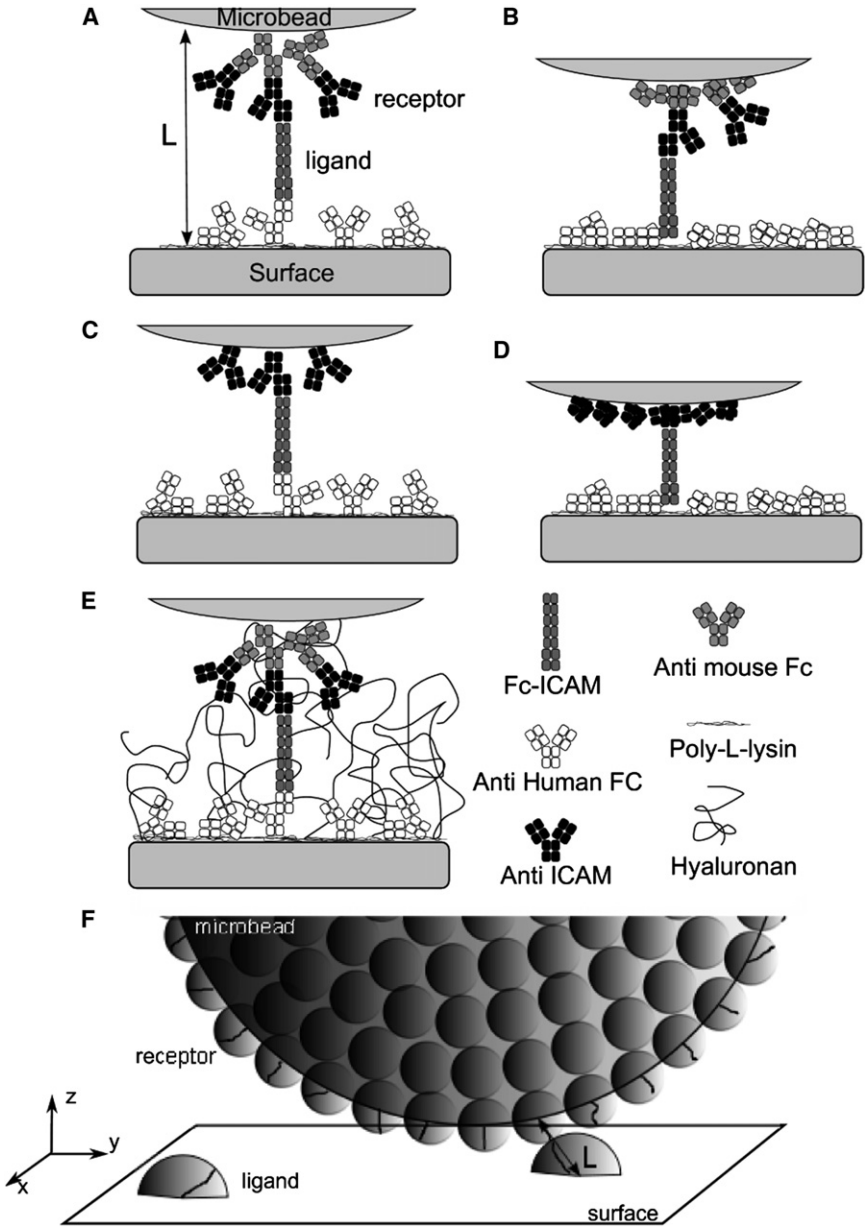

FIGURE 1 (*A–E*) Schematic representation of the different molecular constructions to probe ICAM-1 versus anti-ICAM-1 binding in the laminar flow chamber, at the onset of bond formation. Each square represents an Ig domain of 4 nm. (*A* and *B*) Configuration with a double layer (DL) of antibodies on the bead, with a maximal molecular tether length of $L_{DL} = 76$ nm (*A*) or an intermediate extension tether length of 60 nm (*B*). (*C* and *D*) Configuration with a single layer (SL) of antibodies on the bead, with a maximal molecular tether length of $L_{SL} = 60$ nm (*C*) or an intermediate extension tether length of 44 nm (*D*). (*E*) Configuration *A* in presence of adsorbed hyaluronan molecules acting as a repulsive layer. (*F*) Schematic representation of one microbead at the vicinity of the functionalized surface.

Numerical simulation

The goal of the simulation is to determine the number and duration of encounters between the reactive site of individual receptors immobilized on the microbeads' surface and the reactive site of individual ligands immobilized on the flow chamber floor surface, according to our experimental situation (Fig. 1 *F*). Both receptor and ligand molecules are tethered to either microbead or flow chamber surfaces; reactive sites explore a volume moving with the surface. An encounter occurs when the distance between the anchoring points of an antibody and its ligand on their surfaces is lower than L, the sum of the tether lengths. In the simulation, an encounter starts when the volume swept by a receptor begins to intersect the volume swept by a ligand, and lasts as long as both volumes intersect.

To determine the distribution of encounter durations, we describe in a first step the movement of the microbead surface relative to the chamber floor surface, by calculating the Brownian motion and convection of the microbead in the flow near the floor surface. Input parameters include flow shear rate and microbead-substrate interaction potential, both quantities being experimentally measured and varied. In a second step, we determine the number of encounters and their duration by counting the number and the duration of the intersections of the volumes swept by receptor and ligand reactive sites on their moving surfaces. Receptors and ligands anchoring points are distributed randomly on the surfaces and their average density are measured parameters. Our main assumptions concern the volume swept by the ligand and receptor reactive sites and are based on current knowledge of antibodies and ICAM family structures. For the total tether length L, different values are tested experimentally and numerically. The possible consequences of our assumptions on our results are detailed further in the Discussion.

Brownian dynamics of a bead in flow near a wall

Beads of radius a move in a low Reynolds shear flow which obeys Navier-Stokes equations in their linear approximation. Movements in each spatial

direction (vertical z, horizontal x perpendicular or y parallel to the flow) are then uncoupled. The wall boundary condition on the flow contributes as an additional friction force that slows down the movement of the bead at the vicinity of the wall (23). Translational invariance along the horizontal directions, combined with the absence of coupling between the spatial directions, limits the contribution of the wall to an altitude dependence.

We compute the displacement of the bead by including the convective force of the fluid on the bead, $\vec{F}_{Stokes}$, the thermal force, $\vec{F}_{th}$, and any external force such as the gravity or, more generally, the force that derives from the potential of interaction U between the bead and the wall in absence of ligands, given by $\vec{F}_{int} = -\vec{\nabla}U$. We assume that the movement of the bead is overdamped, and inertia is neglected. As shown in the Supporting Material, the effect of bead rotation is negligible, except for the shear-induced rotation which reduces the velocity of the receptor relative to the ligand, w, compared to the velocity of the center of mass of the bead, V, as $w \simeq 0.43\,V$ (23,24). We therefore focus on the calculation of the velocity of the center of mass of the bead, V, and eventually correct the velocity of the receptor by including rotation effect. Force balance on the bead can be written as

$$\vec{F}_{Stokes} + \vec{F}_{th} + \vec{F}_{int} = \vec{0}. \tag{1}$$

The convective force is calculated using the linearized Navier Stokes equation. Linearity ensures that the hydrodynamic flow is the sum of the unperturbed flow (in absence of the bead), plus the contribution of the force that the bead applies to the fluid, $-F_{Stokes}$. As a result, the velocity of the center of mass of the bead contains the contribution of the unperturbed flow, the coupling between the translational flow and the force field that applies on the bead, and the coupling between the shear flow (gradient of velocity) and the forces that apply on the bead (25) (remember that we neglect couplings between the flow and the rotation of the bead). Replacing the convective force F_{Stokes} by its expression from Newton's law, Eq. 1, the velocity $\vec{V}$ of the center of mass of a hard sphere of radius a reads (16,25)

$$\vec{V} = \begin{pmatrix} \sqrt{D_x(z)}\Gamma_x(t) \\ \sqrt{D_x(z)}\Gamma_y(t) + GaK_v(z) \\ \sqrt{D_z(z)}\Gamma_z(t) - \dfrac{D_z(z)}{k_BT}\dfrac{dU}{dz} \end{pmatrix}, \tag{2}$$

where G is the shear rate. The wall imposes an additional friction (23) accounted for by a damping of the diffusion coefficients, $D_i(z)$, with z the gap between the wall and the bead. $\Gamma_i(t)$ is the i^{th} component of the thermal force normalized by the altitude-dependent diffusion coefficient,

$$\Gamma_i(t) = F^i_{th}(t)/(k_BT)\sqrt{D_i(z)}.$$

K_v is the altitude-dependent correction to the shear velocity that originates from the increased friction of the bead near the wall. Writing

$$D_z(z) = D_0/K_z(z),\ D_x(z) = D_0/K_x(z),\ \text{with}\ D_0 = k_BT/(6\pi\nu a)$$

as the bulk diffusion coefficient in absence of walls and ν the medium viscosity, one has the approximate formulas (24)

$$\begin{aligned} K_z(z) &\simeq \exp\big(0.00577\,\ln(z/a)^3 + 0.0922\,\ln(z/a)^2 \\ &\quad -0.527\,\ln(z/a) + 0.770\big), \\ K_x(z) &\simeq \exp\big(0.00332\,\ln(z/a)^3 + 0.0193\,\ln(z/a)^2 \\ &\quad -0.183\,\ln(z/a) + 0.327\big), \\ K_v(z) &\simeq \exp\big(0.00376\,\ln(z/a)^3 + 0.0723\,\ln(z/a)^2 \\ &\quad +0.548\,\ln(z/a) + 0.689\big). \end{aligned} \tag{3}$$

Langevin Eq. 2 is solved assuming that Γ is a white, Gaussian noise (26): the distribution of the amplitude of the noise is a Gaussian, with its values being time-uncorrelated. Γ verifies

$$\langle\Gamma_i(t)\rangle = 0, \langle\Gamma_i(t)\Gamma_j(t')\rangle = 2\delta_{ij}(t-t'), \tag{4}$$

with no correlation to higher orders. Because there is no correlation time in Eq. 4, and because we have no rule to choose at what time between t and $t+\Delta t$ the altitude-dependent prefactor of the stochastic terms in Eq. 2 should be calculated for its integration, leading to a nonunique result (26). A mathematical definition of the integration rule of Eq. 2 must be specified, and its relevance evaluated in the present physical context, for instance, by looking at the calculated vertical bead distribution under sedimentation. Here, we choose to work in the frame of the Stratonovitch interpretation, which consists of evaluating the stochastic space-dependent terms at time $t+\Delta t/2$ when integrated between t and $t+\Delta t$ (26). This integration rule indeed accounts for a Boltzmann sedimentation profile for the beads above a wall (16).

The numerical integration of Eq. 2 is performed using the Euler algorithm at first order. This algorithm assumes that the coefficients in Eq. 2 have a slower time dependence than the normalized thermal force $\Gamma(t)$ (27). As a consequence,

$$\begin{aligned} \vec{x}(t+\Delta t) - \vec{x}(t) &\simeq \langle\vec{x}(t+\Delta t) - \vec{x}(t)\rangle \\ &\quad + \sqrt{\langle(\vec{x}(t+\Delta t) - \vec{x}(t))^2\rangle}\,\omega, \end{aligned} \tag{5}$$

where ω is a Gaussian-distributed, random number. The first and the second moments in Eq. 5 are calculated by integrating the Langevin equation Eq. 2 using Stratonovitch definition of integrals (26). This results in the following algorithm:

$$\begin{cases} x(t+\Delta t) - x(t) \simeq \sqrt{2D_x(z(t))\Delta t}\ \ \omega_x \\ y(t+\Delta t) - y(t) \simeq GaK_v(z(t))\Delta t + \sqrt{2D_x(z(t))\Delta t}\ \ \omega_y \\ z(t+\Delta t) - z(t) \simeq \left[-\dfrac{D_z(z(t))}{k_BT}\dfrac{dU}{dz} + \dfrac{dD_z}{dz}(z(t))\right]\Delta t \\ \qquad\qquad + \sqrt{2D_z(z(t))\Delta t}\ \ \omega_z \end{cases}. \tag{6}$$

Note the presence of the drift term in the z component of Eq. 6, a consequence of the Stratonovitch integration rule.

Simulation parameters and boundary conditions

A typical run of the simulation consists in generating, for a flow of given shear rate G, the trajectory of $N_b = 200$ beads over a distance of $L_f = 360$ μm, corresponding to the size of the field of view in the microscope. The numerical time step is $\Delta t = 0.001$ ms, chosen to have $v\delta t << 1$ nm, with the bead velocity $v \leq 120$ μm/s. The force of interaction dU/dz is derived from the measured potential $U(z)$ and approximated with the formula

$$\frac{1}{a}\frac{dU}{dz} = A_1 + A_2 e^{-(z-z_0)/z_1},$$

where z is the gap distance between the bead and the wall (see numerical values in Table 1). The initial position of the beads is set to follow the measured bead height distribution $\Phi(z)$, using a rejection method.

Simulation of the duration of molecular encounter

The simulation of ligand-receptor reactive sites encounters relies on several physical assumptions:

Assumption 1. The reactive sites are located at the end of the molecular tether because the variable domain of the antibody binds to the first fragment of ICAM-1.

TABLE 1 Parameters of bead-surface force of interaction as a function of the bead-surface distance *z*

[*HA*] (μg/mL)	A_1 (μN/m)	A_2 (μN/m)	z_1 (nm)	z_0 (nm)
0	−0.1	0.5	17	0
0.02	−0.08	0.5	6	28
0.1	−0.1	0.3	61	43
0.2	−0.2	−0.4	73	134

Note that $(1/a)\ dU/dz = A_1 + A_2 e^{-(z-z_0)/z_1}$ at various hyaluronan concentrations. The value $a = 2.25$ μm is the bead radius.

Assumption 2. Ligands (Fc-ICAM) on the substrate are homogeneously distributed with the measured density σ_L small enough, so that one bead interacts at most with one ligand at a time (see details with the derivation of Eq. S4 in the Supporting Material).

Assumption 3. The density of receptors (anti-ICAM) on the bead is sufficiently high (measured at 300 molecule/μm^2 (14)), so that virtually all points of the bead are actually bearing a receptor.

Assumption 4. Reactive sites at the end of a molecular tether explore rapidly the surface of a sphere, the radius of which is given approximately by the maximal extension of the tether. The extension is determined by the high rotational freedom of the antibody hinges combined with relative rigidity of immunoglobulin domains (see the Supporting Material). Consequently, one encounter starts as soon as the distance d between the anchoring points of a free ligand and a free receptor is equal or less than L, the total molecular tether extension.

Assumption 5. Once established, the contact between reactive sites is maintained against diffusion of the tethers due to an energetically favorable conformation. Consequently, a ligand-receptor encounter holds until the receptor is brought out of the interaction range $d > L$, due to the bead displacement.

Assumption 6. Finally, the bead arrests are not included in the simulation; these rare events do not affect significantly the distribution of encounter durations calculated in the absence of arrests. The frequency of arrests is calculated in a next step (see Results), using the analytical expression Eq. 7 that relates the distribution of encounter durations to the frequency of arrests for an energy profile as plotted later in Fig. 6.

Assumptions 4 and 5 will be further addressed in the discussion.

Following these assumptions, simulations compute the trajectories of Brownian beads in a shear flow, with diffusion coefficients accounting for the experimental profile of energy of interaction with the wall (Eq. 6). The bead is considered to encounter a ligand for the first time if there is an overlap between the interaction regions of a ligand on the wall and a receptor on the bead at time $t + \Delta t$, but no overlap at time t.

To save computing time, the distribution of ligands is not computed but a sliding-carpet approach is used instead: at each time step of the simulated bead motion, if no encounter is occurring yet, a ligand is randomly positioned on the surface at a distance of the center of the bead that is larger than $a + L$ at time t, and lower than $a + L$ at time $t + \Delta t$. Next, the probability of interaction between this randomly chosen ligand and the bead is evaluated as $p = \sigma_L S$, with $\sigma_L = 2$ molecules/μm^2 the measured density of ICAM ligands on the surface, and S the surface of the interaction region between the ligand and the bead at time $t + \Delta t$, excluded of the interaction region at time t (see the Supporting Material and Fig. 2 for a detailed calculation of the surface, S). A random number is picked in a homogeneous distribution between 0 and 1, and its value is compared to p.

It determines whether an interaction indeed occurs between this specific ligand and some receptor on the bead. The location of the first interacting receptor on the bead is randomly picked in the zone fulfilling $d \leq L$, with d the distance between the ligand and the receptor anchoring points. The duration of encounter t_e is defined as the time during which this distance d is equal or less than L. After detachment of the first interacting receptor, the location of the next interacting receptor with the same ligand is randomly chosen on the bead surface, with the condition $d \leq L$. Another choice for the next receptor, within $d \leq L$, does not affect significantly our results (see the Supporting Material). The encounter ends when no more receptor can interact with this specific ligand. We checked on several examples that use of a random predetermined distribution of ligands on the substrate gives the same result as the sliding carpet approach.

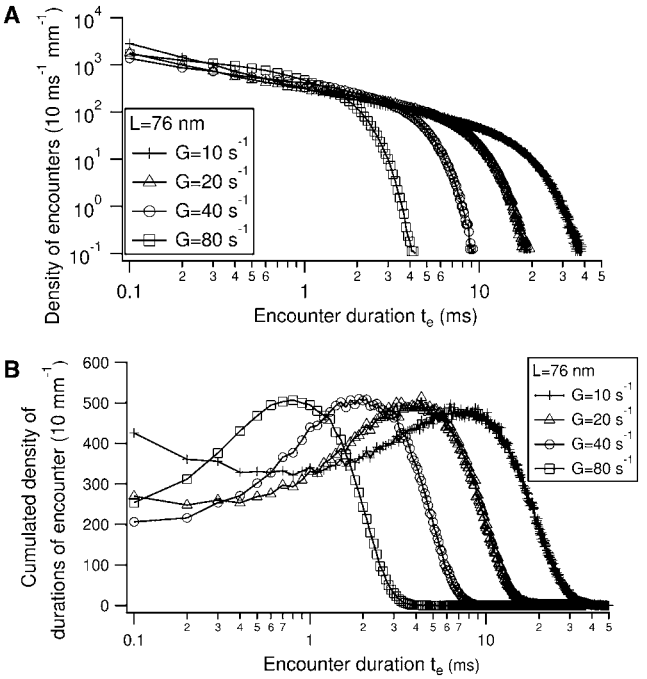

FIGURE 2 Numerical simulation of ligand-receptor encounters in the flow chamber. (*A*) Density of encounter durations $q_{G,L}(t_e)$ per traveled distance of the bead and per $\Delta t_e = 0.1$ ms time bins. G is the imposed flow shear rate and L is the total molecular tether length separating the reactive sites from the anchoring points on the surfaces. (*B*) Cumulated density $q_{G,L}(t_e).t_e$.

RESULTS

Number and duration of molecular encounters

We first study the situation in the absence of the glycocalyx mimicking layer of hyaluronan, where the most probable height of the bead is measured around z_0 ~25 nm. The distribution of velocities retrieved from simulation of sedimented beads is consistent with the measured distribution. It exhibits a peak of velocity proportional to the shear rate,

$$V_{max} \simeq 0.54aG \simeq aGK_v(z_0),$$

which is used to deduce the imposed shear rate from the experimental peak velocity.

The density of encounter durations $q(t_e)$ is defined as the number of molecular encounters per bead and per millimeter along the flow, which have a duration between t_e and $t_e + \Delta t_e$.

For shear G and molecular tether length L, $q_{G,L}(t_e)$ exhibits high values at vanishing encounter durations, representing encounters limited by the diffusion of the bead (Fig. 2 *A*). Then the density decays rapidly for higher durations, corresponding to encounters limited by the bead convection. The cumulated density $q(t_e) \cdot t_e$ (Fig. 2 *B*) displays a maximum which occurs at long encounter duration, this duration varying as the inverse of the shear rate.

Frequency of adhesion for variable shear rates

Writing $P(t_e)$ the probability of forming a bond after an encounter of duration t_e, the frequency of adhesion $FA(G, L)$ is

$$FA(G,L) = \sum_{t_e=0}^{t_{max}} q_{G,L}(t_e)P(t_e)\Delta t_e. \quad (7)$$

Here, t_{max} represents the maximal encounter duration which can be reached experimentally, as visualized in Fig. 2. As detailed previously (14), we propose that $P(t_e)$ is partly set by the diffusion of the reactive complex on a unidimensional rough energy landscape, along a certain reaction coordinate (28). Let t_{on} be the typical time to diffuse from the entry of the energy landscape to the first barrier or well representing the measured bound state. $P(t_e)$ is calculated as a first-passage problem and is proportional to

$$\mathrm{erfc}\sqrt{(t_{on}/t_e)}$$

after integration of the equation of diffusion. Introducing the proportion coefficient α, whose significance will be discussed later, we write:

$$P(t_e) = \alpha\ \mathrm{erfc}\sqrt{(t_{on}/t_e)}. \quad (8)$$

Parameters α and t_{on} are estimated as follows. Adhesion of beads coated with a double layer of antibodies (DL configuration) on a Fc-ICAM coated substrate (density $\sigma_L = 2$ molecules/μm^2) in absence of hyaluronan, has been measured for variable shear rates G. The frequency of adhesion as a function of the inverse of the shear rate is represented as black points in Fig. 3 *A*. For each experimental shear rate G and molecular tether length L, the numerical simulation provides a density of encounter duration $q_{G,L}(t_e)$, as exemplified on Fig. 2. Using Eq. 7, the predicted $FA(G, L)$ is calculated to fit the experimental points, by adjusting the two free parameters α and t_{on}. Experimental data with optimal fit are shown on Fig. 3 *A*. When L is varied, different values of the fitting parameters are obtained (Fig. 3 *B*), which give insight about the precision of our fitting parameters, taking into account the uncertainty in the tether length L. For three possible values of $L_{DL} = 76$, 60, and 44 nm in the DL configuration, one finds respectively $t_{on} = 7$, 6, and 4 ms.

As an alternative to the hypothesis of a minimal time for bond formation, one can assume the existence of the classical on-rate constant k_{on} for binding, writing the binding probability as

$$P_1(t_e) = 1 - \exp(-k_{on}t_e).$$

Inserting P_1 in Eq. 7 and taking k_{on} as a free parameter, the best fit of experimental frequency of adhesion is shown as the straight dashed line on Fig. 3 *A*. Using alternatively the probability

$$P_2(t_e) = \frac{k_{on}}{k_{on} + 1/t_e}$$

(as in Chang and Hammer (15)) gives an identical line, incompatible with our measurements. Because the fit in these two cases is linear,

$$P_1(t_e) \simeq P_2(t_e) \simeq k_{on}t_e$$

and one determines

$$k_{on} = 0.048, 0.065\ \mathrm{s}^{-1}$$

for $L = 76$, 60 nm, respectively. Taking the maximal encounter time $t_{max} \simeq 50$ ms as estimated from Fig. 2 *A*, one has

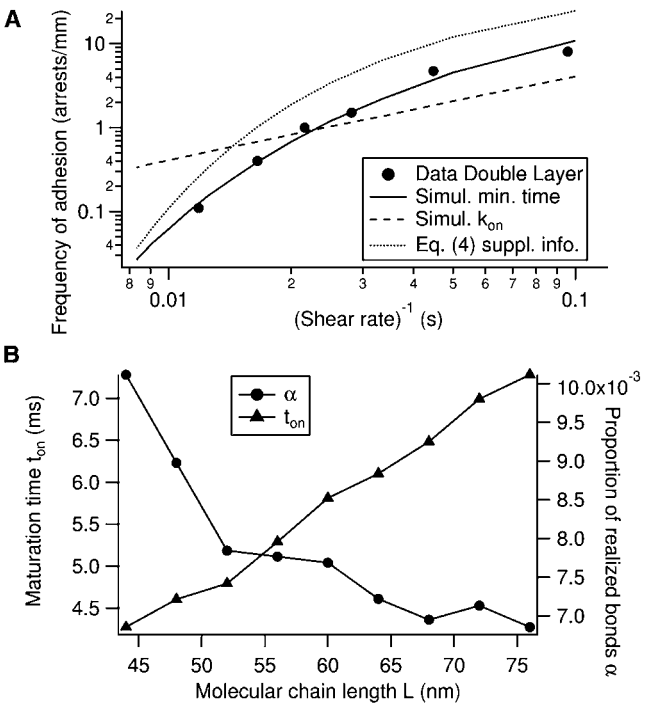

FIGURE 3 (*A*) Fit of experimental frequency of adhesion as function of inverse of shear rate G (*solid line*), using the hypothesis of a minimal binding time t_{on} and for the molecular tether length $L = 60$ nm (choice of $L = 76$ nm or $L = 44$ nm give identical fit). (*Dotted line*) Eq. S4 of the Supporting Material with coefficients t_{on} and α obtained with the former fit. (*Dashed line*) Result of fitting assuming the classical hypothesis of an on-rate coefficient k_{on} and $L = 60$ nm. (*B*) Variation of the fitted parameters α and t_{on} with L .

$$k_{on} \cdot t_{\max} \ll 1,$$

which confirms the linear regime for P_1 and P_2. In this limit, k_{on} can be factorized in Eq. 7 and the binding probability is proportional to the area under the curve in Fig. 2 *B*.

Effect of molecular tether length

The frequency of arrests (FA) was measured using beads coated with a single layer of antibodies on the bead (SL configuration). Predicted FA was obtained by taking, for α and t_{on}, the reference values determined with two layers of antibodies on the beads (DL configuration, see previous section) and by calculating the distribution of encounter durations for L estimated for the SL configuration. Measured and calculated FA show a satisfactory agreement for the molecular tether length $L_{DL} \simeq 60$ nm (Fig. 4). As a comparison, we calculated the predicted adhesion frequency in the classical approach of k_{on}, using the fitted value obtained previously in the double-layer configuration (Fig. 3 *A*). The result is represented in Fig. 4 as a thin dashed line.

Effect of a glycocalyx-like repulsive layer

The interaction potential between the bead and the substrate was modified by addition of a repulsive layer of hyaluronan on the substrate at variable polymer surface densities. Interaction force was measured for shear $G \simeq 0$–$10\ s^{-1}$ and the corresponding height distribution used in the simulation is shown in Fig. 5, *A* and *B*. Numerical parameters extracted from the fit of the measured force are given in Table 1. Measured and predicted frequencies of adhesion are shown in Fig. 5 *C*. Although a correct agreement between measurement and prediction is obtained at low surface densities, a significant discrepancy is observed for concentrations exceeding 0.1 μg/mL, probably reflecting heterogeneities of the polymer layer, as discussed below.

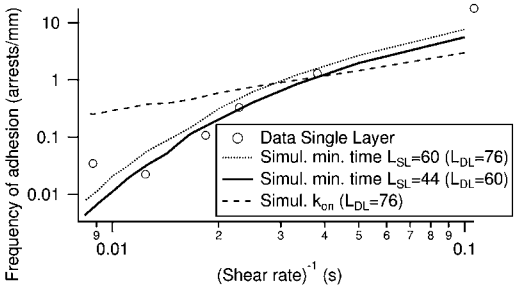

FIGURE 4 Frequency of adhesion as function of inverse of shear rate G for molecular construction involving a single layer of antibodies on the bead (SL configuration). Simulations with the minimal binding time hypothesis are realized by taking as molecular tether length $L_{SL} = 60$ or 44 nm (corresponding respectively to $L_{DL} = 76$ or 60 nm with two layers of antibodies on the beads) and the parameters t_{on} and α obtained previously in Fig. 3. (*Thin dashed line*) Simulation with the classical hypothesis of k_{on} and $L_{SL} = 60$ nm.

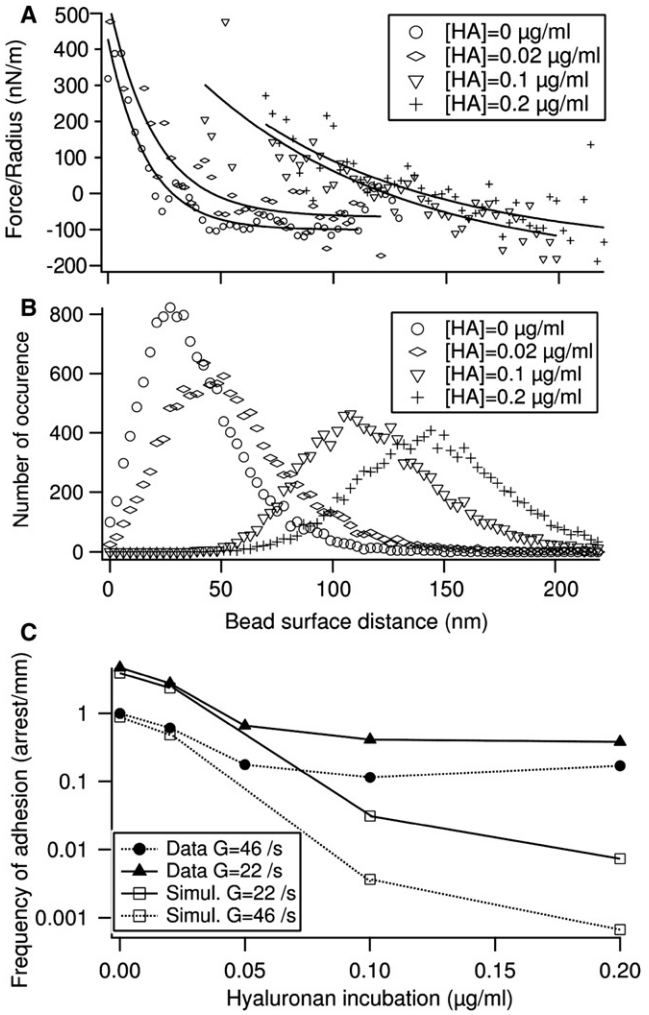

FIGURE 5 Effect of a glycocalyx-like coating. (*A*) Measured interaction force between bead and substrate, normalized by the bead radius, for various coating densities of hyaluronan. (*Solid lines*) Fits. (*B*) Distribution of bead surface distance used in the simulation and corresponding to the force fits shown in panel *A*. (*C*) Comparison of measured and predicted frequencies of adhesion in presence of variable amount of hyaluronan repulsive layer, taking $L = 76$ nm in the simulation.

DISCUSSION

Although antibodies often bind to antigens in a soluble form, binding also occurs when antibodies are bound to the cell surface (9).

A first example concerns surface-bound antibodies of B lymphocytes: capture of their antigens can start B-lymphocyte activation and antibody production. Additionally, this event may require intervention of T lymphocytes, which depends on the binding characteristics of the antigen to the B lymphocyte through their surface antibodies.

A second example involves mastocytes and basophil polymorphonuclear cells which express antibody receptors with a very high affinity to the IgE antibody class. Hence, IgE are bound to these receptors before encountering their ligands. Ligand-binding triggers cell activation that starts an inflammatory reaction. This inflammatory reaction has an important physiological role as it is the beginning of anti-parasitic immune reactions, and an important pathological role as it is the cause of most allergic symptoms. Therefore, quantification of bond formation in surface-bound conditions is necessary to understand the characteristics of bonds between antibodies and pathogenic antigens.

In this study, we examined the dependence of the binding efficiency on the duration of interaction between ligand and receptor bound to surfaces, taking the antigen-antibody bond as a model interaction. Different ways have been used to modulate this duration:

1. Systematic variation of the velocity of the beads along the surface by increasing the shear rate; this situation was already studied theoretically by Chang and Hammer (15): similarities and differences with our approach are detailed in the Supporting Material.
2. Reduction of the molecular tether length.
3. Increasing of the surface distance by addition of an adsorbed polymer layer of HA.

We showed that the frequency of adhesion can be written as an integral formula (Eq. 7) featuring the simulated distribution of ligand-receptor encounter duration and two measured parameters α and t_{on} characterizing the molecular binding properties of the Fc-ICAM/anti-ICAM complex. A physical interpretation of t_{on} is that it represents the typical diffusion time on a rough energy landscape (14), represented in Fig. 6. As shown in Fig. 3 *B*, t_{on} varies linearly with the molecular tether length L. This illustrates the fact that, although this quantity represents an intrinsic characteristic of the molecular complex formation, its measurement depends on a correct knowledge of the molecular tether length. For the most realistic choice of $L = 60$ nm, we determine $t_{on} \simeq 6$ ms. We show in the Supporting Material that this estimate of L is reasonable due to the structure of the antibodies used as tethers, which combine high rotational freedom while keeping an end-to-end distance close to the maximal extension.

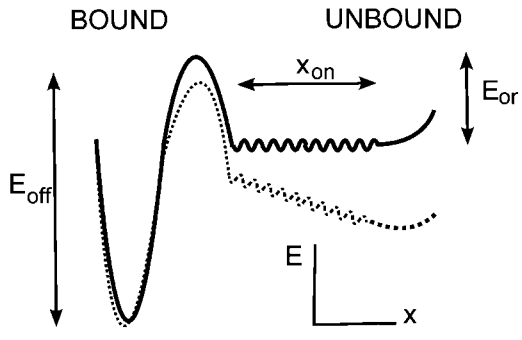

FIGURE 6 Putative energy landscape summarizing the binding properties of the Fc-ICAM/anti-ICAM complex. In the absence of external force (*solid line*), binding occurs by successive crossing of a rough flat landscape of extension $x_{on} \simeq \sqrt{D_{on} t_{on}}$ and a barrier of height $E_{on} \simeq -k_B T \ln \alpha$. A slight depression at the entrance of the landscape keeps reactive sites together against tether conformational change. With a moderate external force applied on the tethers (*dashed line*), complexes in the rough landscape detach immediately. Complexes in the deep minimum detach with an off-rate $k_{off} \sim \exp(-E_{off}/k_B T)$, quasiindependent of the applied force. The values α and t_{on} are the parameters measured in this study.

We propose that the parameter α represents the fraction of mature complexes (i.e., those which result from molecular encounter longer than t_{on}) which effectively form a detectable bond. We propose that α reveals the presence of an internal energy barrier, as illustrated in Fig. 6. Regarding the value of α, the height of the barrier would be

$$E_{on} \simeq -k_B T \ln \alpha \simeq 5\, k_B T.$$

An interesting observation is that α is weakly dependent on L in the range 60–76 nm (Fig. 3 *B*). This observation indicates that this quantity may represent a more internal feature in the landscape than t_{on}, which further supports the interpretation that α could originate from states of energy that are intrinsic to the formation of the bond. Other interpretations of the parameter α could in principle be considered:

First, only a small fraction of ligands is able to form a bond: this is unlikely because we measure directly the density of functional ligands by counting the binding of a soluble antibody, identical to the receptor coating the beads and being fluorescently labeled.

Second, an incorrect calculation of the distribution q in Eq. 7; to discard this possibility, we justify further our Assumptions 4 and 5 in the simulation, as formulated in Materials and Methods. Assumption 4 states that reactive site encounters occur as soon as interaction spheres of total radius L intersect; this supposes that tether conformations are explored rapidly. The corresponding timescale t_{conf} can roughly be estimated by considering the free diffusion on distance L of a domain of size d:

$$t_{conf} = \frac{6\pi\nu d L^2}{kT}.$$

With $L = 60$ nm and $d = 4$ nm, one obtains $t_{conf} \sim 60\ \mu$s, much lower than the millisecond-long encounter duration. To fulfill Assumption 5 of the simulation, we have introduced a slight depression at the entrance of the energy landscape (Fig. 6) to represent the fact that the initial encounter can resist tether movements. This is reasonable because it has been shown, in particular for antigen-antibody reaction, that hydrodynamic or electrostatic steering may indeed enforce and stabilize immature reactive site encounters (29,30). The value of α we obtain is ~0.01, corresponding to a quite high barrier of potential, of 5 $k_B T$. Although some antibodies may attach more efficiently, and may

correspond to larger values of α, on-rates measured in solution (as in Schwesinger et al. (31)) can vary by approximately two orders of magnitude, therefore compatible with $\alpha \simeq 0.01$.

Varying the length of the tether led us to the observation that the frequency of adhesion is roughly approximated by the product of two terms, when the convection of the beads dominates over diffusion (see Eq. S4 in the Supporting Material): the density of encounters per unit length, λ, and the probability of bond formation,

$$\alpha \ \mathrm{erfc}\sqrt{\left(t_{on}/t_e^*\right)}.$$

The value λ can be understood as the product of the number of ligands of the surface encountered by the bead per unit length of trajectory multiplied by the number of receptors of one bead interacting with the same ligand. The value λ depends only on the geometry of the experiment through the following parameters: bead radius a, molecular tether length L, typical bead height z_0, and ligand density on the surface σ_L. The value t_e* is the typical encounter duration imposed by the convection of the bead.

Recently, Fc-ICAM has been used as a model of dimer to study the recognition with β_2 integrins (32). Indeed, it was recognized that monomeric and dimeric ICAMs exhibit different cell activation properties. However, a systematic comparison in an acellular system is still missing. In our case, we believe that the recognition of ICAM by the anti-ICAM antibody is not affected by the monomeric or dimeric configuration, and that the proposed mechanism applies for antibody recognition of monomers. In support of this, preliminary results obtained with antibodies binding to a monomeric major histocompatibility complex exhibits also a minimal duration required for binding.

With a hyaluronan coat, the prediction of the adhesion frequency obtained from the simulation fails to reproduce the measurements obtained at HA incubation concentrations exceeding 0.1 μg/mL, corresponding to a most probable height higher than 90 nm. This can be explained in part by the limited precision in the measurement of the hyaluronan layer with RICM. Additionally, our simulation assumes a uniform hyaluronan cushion, the density being dependent only on the distance to the substrate z. The observed discrepancy may arise from the possible heterogeneity of the cushion and the presence of thinner zones in the cushion which allow an access to the ICAM ligand, resulting in a higher adhesion frequency.

This is supported by the occasional observation that, during beads height measurement with RICM, some beads may reach the surface and eventually stick to it, even in the presence of a high amount of hyaluronan. Accounting properly for such lateral heterogeneity is not accessible to our simulation, where the bead-surface potential depends only on the z coordinate. Compensating for this spatial dependence by improving the description of the short-range bead-surface interaction ($<$10 nm) may not be sufficient. Finally, we have reported earlier a slight increase in apparent viscosity next to the wall due to dense hyaluronan coats (19,33,34); however, as shown in Robert et al. (19), convection remains unchanged in presence or absence of hyaluronan. As convection, rather than diffusion, of the bead limits encounter duration, we do not expect a significant impact on our results.

In conclusion, we have shown that a new description of the association kinetics may be required in the case of surface-attached molecules, as exemplified on the antibody-antigen example. Although the energy landscape established from our study should, in principle, also hold for soluble molecules, there is (to our knowledge) no experimental procedure to explore this. Our assumptions are compatible with the usual conception that antigen-antibody reactions in solution are diffusion-limited (9). However, as mentioned in the Introduction, comparison of soluble and surface-bound kinetics is rendered difficult by the possible existence of multiple bound states.

Hence, on-rate measured in solution may appear faster if it involves one bound state near the entrance of the energy landscape, which is not detectable with the laminar flow chamber. Introducing a minimal time necessary for bond formation, we can quantitatively account for the effect of the molecular environment on the bond formation, a critical question rarely addressed at the single molecule level. The generality of this mechanism is supported by preliminary observations concerning other ligand-receptor bonds involved in immunological functions. Interesting perspectives arise concerning the consequences of this mechanism when involving membrane-diffusible molecules and the regulation of cell adhesion and signaling.

SUPPORTING MATERIAL

Additional text with two figures and four equations is available at http://www.biophysj.org/biophysj/supplemental/S0006-3495(11)00420-6.

We thank Pierre-Henri Puech for numerous discussions and Kheya Sengupta for careful reading of the manuscript.

We thank Agence Nationale de la Recherche for financial support under "ADHEKON" grant No. JCJC06-0135.

REFERENCES

1. Bongrand, P. 1999. Ligand-receptor interactions. *Rep. Prog. Phys.* 62:921–968.
2. Merkel, R., P. Nassoy, …, E. Evans. 1999. Energy landscapes of receptor-ligand bonds explored with dynamic force spectroscopy. *Nature.* 397:50–53.
3. Pierres, A., H. Feracci, …, P. Bongrand. 1998. Experimental study of the interaction range and association rate of surface-attached cadherin 11. *Proc. Natl. Acad. Sci. USA.* 95:9256–9261.
4. Chesla, S. E., P. Selvaraj, and C. Zhu. 1998. Measuring two-dimensional receptor-ligand binding kinetics by micropipette. *Biophys. J.* 75:1553–1572.

5. Huppa, J. B., M. Axmann, …, M. M. Davis. 2010. TCR-peptide-MHC interactions in situ show accelerated kinetics and increased affinity. *Nature*. 463:963–967.
6. Robert, P., L. Limozin, …, P. Bongrand. 2006. Glycocalyx regulation of cell adhesion. *In* Principles of Cellular Engineering: Understanding the Biomolecular Interface.. Elsevier Academic Press, Amsterdam, The Netherlands. 213–231.
7. Huang, J., J. Chen, …, M. Long. 2004. Quantifying the effects of molecular orientation and length on two-dimensional receptor-ligand binding kinetics. *J. Biol. Chem.* 279:44915–44923.
8. Jeppesen, C., J. Y. Wong, …, C. M. Marques. 2001. Impact of polymer tether length on multiple ligand-receptor bond formation. *Science.* 293:465–468.
9. Murphy, K., and M. W. P. Travers. 2008. Janeway's Immunobiology. Garland Publishing, New York.
10. Robert, P., A.-M. Benoliel, …, P. Bongrand. 2007. What is the biological relevance of the specific bond properties revealed by single-molecule studies? *J. Mol. Recognit.* 20:432–447.
11. Bell, G. I. 1978. Models for the specific adhesion of cells to cells. *Science.* 200:618–627.
12. Pincet, F., and J. Husson. 2005. The solution to the streptavidin-biotin paradox: the influence of history on the strength of single molecular bonds. *Biophys. J.* 89:4374–4381.
13. Marshall, B. T., K. K. Sarangapani, …, C. Zhu. 2005. Force history dependence of receptor-ligand dissociation. *Biophys. J.* 88:1458–1466.
14. Robert, P., L. Limozin, …, P. Bongrand. 2009. Biomolecule association rates do not provide a complete description of bond formation. *Biophys. J.* 96:4642–4650.
15. Chang, K. C., and D. A. Hammer. 1999. The forward rate of binding of surface-tethered reactants: effect of relative motion between two surfaces. *Biophys. J.* 76:1280–1292.
16. Korn, C. B., and U. S. Schwarz. 2007. Mean first passage times for bond formation for a Brownian particle in linear shear flow above a wall. *J. Chem. Phys.* 126:095103.
17. Beste, M. T., and D. A. Hammer. 2008. Selectin catch-slip kinetics encode shear threshold adhesive behavior of rolling leukocytes. *Proc. Natl. Acad. Sci. USA.* 105:20716–20721.
18. Schmidt, B. J., J. A. Papin, and M. B. Lawrence. 2009. Nano-motion dynamics are determined by surface-tethered selectin mechanokinetics and bond formation. *PLOS Comput. Biol.* 5:e1000612.
19. Robert, P., K. Sengupta, …, L. Limozin. 2008. Tuning the formation and rupture of single ligand-receptor bonds by hyaluronan-induced repulsion. *Biophys. J.* 95:3999–4012.
20. Paul, W. 2008. Fundamental Immunology. Lippincott Williams and Wilkins, New York.
21. Limozin, L., and K. Sengupta. 2009. Quantitative reflection interference contrast microscopy (RICM) in soft matter and cell adhesion. *ChemPhysChem.* 10:2752–2768.
22. Sengupta, K., J. Schilling, …, E. Sackmann. 2003. Mimicking tissue surfaces by supported membrane coupled ultrathin layer of hyaluronic acid. *Langmuir.* 19:1775–1781.
23. Goldman, A. J., R. Cox, and H. Brenner. 1967. Slow viscous motion of a sphere parallel to a plane wall. II. Couette flow. *Chem. Eng. Sci.* 22:653–660.
24. Pierres, A., A. M. Benoliel, …, P. Bongrand. 2001. Diffusion of microspheres in shear flow near a wall: use to measure binding rates between attached molecules. *Biophys. J.* 81:25–42.
25. Cichocki, B., and R. Jones. 1998. Image representation of a spherical particle near a hard wall. *Physica A.* 258:273–302.
26. Kampen, N. V. 2007. Stochastic Processes in Physics and Chemistry, 3rd Ed. North-Holland, Amsterdam, The Netherlands.
27. Gardiner, C. W. 1985. Handbook of Stochastic Methods, 3rd Ed. Springer-Verlag, London, UK.
28. Zwanzig, R. 1988. Diffusion in a rough potential. *Proc. Natl. Acad. Sci. USA.* 85:2029–2030.
29. Brune, D., and S. Kim. 1994. Hydrodynamic steering effects in protein association. *Proc. Natl. Acad. Sci. USA.* 91:2930–2934.
30. Kozack, R. E., M. J. d'Mello, and S. Subramaniam. 1995. Computer modeling of electrostatic steering and orientational effects in antibody-antigen association. *Biophys. J.* 68:807–814.
31. Schwesinger, F., R. Ros, …, A. Pluckthun. 2000. Unbinding forces of single antibody-antigen complexes correlate with their thermal dissociation rates. *Proc. Natl. Acad. Sci. USA.* 97:9972–9977.
32. Evans, E., K. Kinoshita, …, A. Leung. 2010. Long-lived, high-strength states of ICAM-1 bonds to $\beta 2$ integrin. I. Lifetimes of bonds to recombinant alphaLbeta2 under force. *Biophys. J.* 98:1458–1466.
33. Limozin, L., and K. Sengupta. 2007. Modulation of vesicle adhesion and spreading kinetics by hyaluronan cushions. *Biophys. J.* 93:3300–3313.
34. Sengupta, K., and L. Limozin. 2010. Adhesion of soft membranes controlled by tension and interfacial polymers. *Phys. Rev. Lett.* 104:088101.